Review

Not peer-reviewed version

Recent Advances in FIB-SEM for Microstructural Characterization of Metallic Materials

Yi Qiao * and Yong Zhang *

Posted Date: 23 March 2026

doi: 10.20944/preprints202603.1683.v1

Keywords: focused ion beam-scanning electron microscopy (FIB-SEM); multimodal correlative characterization; metallic material characterization

 doi:10.20944/preprints202603.1683.v1

Review

Recent Advances in FIB-SEM for Microstructural Characterization of Metallic Materials

Yi Qiao * and Yong Zhang *

State Key Laboratory for Advanced Metals and Materials, University of Science and Technology Beijing, Beijing, China

* Correspondence: qiaoyi@ustb.edu.cn (Y.Q.); drzhangy@ustb.edu.cn (Y.Z.)

Abstract

Since its introduction, focused ion beam (FIB) technology has expanded from micro/nanofabrication in the semiconductor industry into the field of multimodal characterization of metallic material microstructures. This article systematically reviews the latest research advances of FIB-SEM technology in the field of metallic materials science. The fundamental principles and system functions of FIB-SEM are introduced, with emphasis on its key applications in two-dimensional and three-dimensional morphological characterization, as well as specimen preparation for transmission electron microscopy (TEM) and atom probe tomography (APT). The combined strategies of FIB-SEM with electron backscatter diffraction (EBSD), time-of-flight secondary ion mass spectrometry (TOF-SIMS), and other characterization techniques are also discussed. Current developments indicate that FIB-SEM technology is advancing toward multi-ion-source synergy and multimodal integration. In the future, combined with artificial intelligence and big data analysis, it is expected to enable high-throughput, correlative measurements of multidimensional properties at the micro-scale, providing important technical support for "materials genome" research in metallic materials.

Keywords: focused ion beam-scanning electon microscopy (FIB-SEM); multimodal correlative characterization; metallic material characterization

1. Introduction

Since the advent of the FIB-SEM dual-beam system (1988, P. Sudraud and G. Ben Assayag) [1], the combined system of a focused ion beam (FIB) and scanning electron microscope (SEM)—the FIB-SEM dual-beam system—has become the mainstream platform for FIB technology applications. In this system, the SEM and FIB can both be focused on the same region of interest on a material: the SEM provides imaging and positioning while the FIB performs ion-beam machining. The application of FIB has thus expanded beyond semiconductors to materials science, geology, biology, and other fields, where it has flourished [2–4].

2. Principles of FIB-SEM

2.1. FIB

A typical FIB instrument comprises a vacuum system and chamber, ion source, ion-optical column, specimen stage, detectors, gas injection system, and control system [5]. The ion source is the key component of any FIB system; the liquid metal ion source using gallium (Ga) was the origin of practical FIB technology. Modern FIB systems have since been developed using a variety of ion species, including helium (He), neon (Ne), gallium (Ga), argon (Ar), and xenon (Xe). Based on the ion-source operating principle, FIB systems can be classified into liquid metal ion source (LMIS) systems, gas field ionization source (GFIS) systems, and plasma ion source systems.

 doi:10.20944/preprints202603.1683.v1

LMIS (Liquid Metal Ion Source): Operating principle—field evaporation of a liquid metal. Ion types—metal ions (Ga^+, Bi^+). Beam spot size—relatively small (~5 nm). Beam current—moderate to high (10^0–10^2 nA). Typical applications—general-purpose FIB machining, circuit editing, TEM specimen preparation, and nanoscale deposition.

GFIS (Gas Field Ionization Source): Operating principle—field ionization of a gas-phase atom. Ion types—gas ions (He^+, Ne^+). Beam spot size—extremely small (<0.5 nm). Beam current—relatively low (10^0–10^2 pA). Typical applications—helium/neon ion microscopy for ultra-high-resolution imaging and nanoscale patterning.

Plasma Ion Source: Operating principle—plasma generated by gas discharge. Ion types—gas ions (Xe^+, Ar^+). Beam spot size—relatively large (>10 nm). Beam current—large (10^2–10^3 nA). Typical applications—rapid, high-throughput specimen preparation and deep etching (e.g., three-dimensional tomography).

2.2. FIB-SEM

The FIB-SEM system integrates FIB and SEM into a single vacuum chamber, combining nanoscale machining (FIB) with high-resolution imaging (SEM). In an FIB-SEM system, the FIB ion column and the SEM electron column are typically arranged at an angle of 36°–38° to each other. During operation, the FIB ion column is usually oriented perpendicular to the material being processed or characterized, as shown in Figure 1. The specimen stage of an FIB instrument is a precision multi-degree-of-freedom motion system. Its core motion capabilities include standard X, Y, and Z orthogonal linear translations (forming a Cartesian coordinate system), together with integrated rotational and tilt degrees of freedom for complex attitude adjustment.

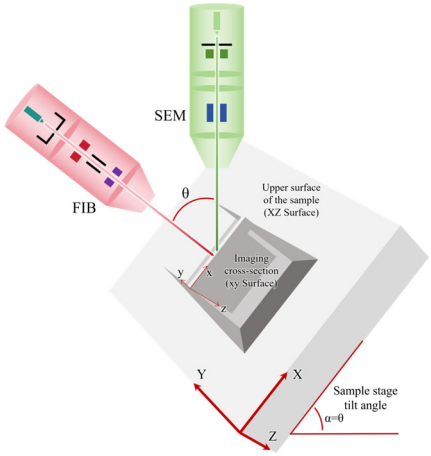

Figure 1. Schematic of FIB-SEM specimen processing.

The interaction behaviors between FIB-SEM and material atoms can be divided into those of the ions from the FIB column and those of the electrons from the SEM column, as shown in Figure 2a.

Ion–atom interactions in FIB: Incident ions undergo elastic and inelastic collisions with atoms in the material, producing elastic and inelastic scattering, respectively. Elastic collisions transfer energy from the incident particle to material atoms, triggering a cascade of secondary collisions. Some incident ions are backscattered at the material surface and leave as backscattered ions. Other incident ions, through the collision cascade, knock material atoms from their lattice sites toward the surface, creating recoil atoms. When a recoil atom has sufficient energy to overcome the surface binding energy, it is ejected from the material as a sputtered particle. Some charged sputtered particles become secondary ions (SI) after further ionization; these signals can be collected by a detector and used for imaging. The inelastic collision channel also excites plasmons and phonons while producing a large number of secondary electrons (SE), whose signals can likewise be collected and used to form images.

 doi:10.20944/preprints202603.1683.v1

Electron–atom interactions in SEM: Incident electrons undergo elastic and inelastic scattering with material atoms. Elastic scattering causes large-angle deflection of electrons, generating backscattered electrons (BSE) whose yield is related to atomic number and can be used for compositional analysis. Backscattered electrons originating from a certain depth within a crystalline material, when satisfying the Bragg diffraction condition, produce characteristic Kikuchi diffraction patterns that can be used to analyze crystal orientation, phase, and strain (EBSD). Inelastic scattering transfers energy to the specimen, producing multiple signals: excitation of low-energy secondary electrons from the near-surface region forms the basis of morphological imaging (SE image); excitation of inner-shell electrons generates characteristic X-rays for elemental analysis (EDS); Auger electrons and cathodoluminescence are also produced. These signals originate from different depths within the specimen surface and together constitute the multifunctional platform of SEM for high-resolution imaging, micro-area compositional analysis, and crystal structure and orientation analysis.

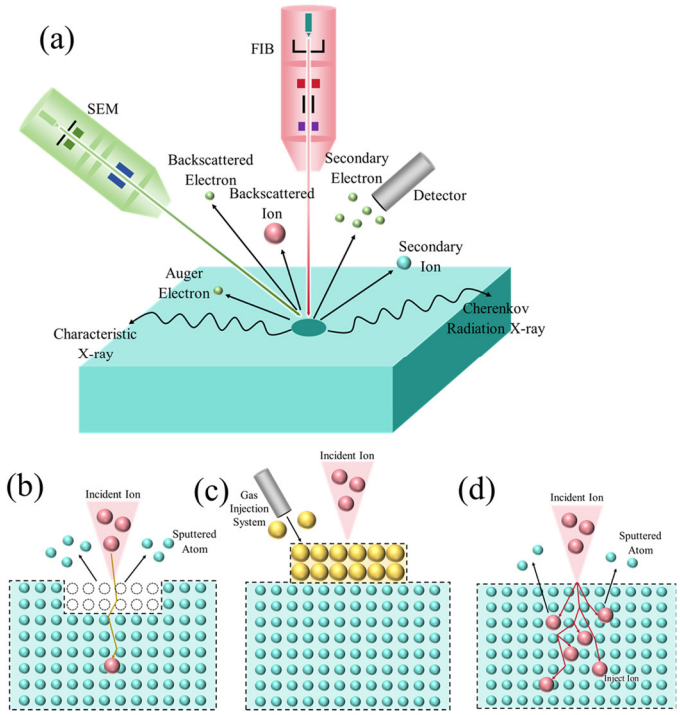

Figure 2. Schematic of the basic functions of a focused ion beam system: (a) scanning imaging; (b) sputter etching; (c) induced deposition; (d) ion implantation.

When a focused ion beam scans the specimen surface, it excites secondary electron (SE) and secondary ion (SI) signals that can be collected by various detectors equipped on the FIB system. Most FIB systems are equipped with a gas injection system; combined with SiO_2, Pt, Au, W, and C gas precursors, they can realize ion-beam-assisted induced deposition for material surface protection and nano-device assembly. Combined with XeF_2 gas, assisted etching of silicon is possible; combined with H_2O gas, assisted diamond etching can be performed. Consequently, the functions of a focused ion beam system include ion exposure, ion implantation, ion etching, elemental deposition, integrated circuit fabrication, and mask repair [6–10], as shown in Figure 2.

Based on the above interactions of particles with material atoms in both FIB and SEM, the functions of FIB-SEM can be summarized to include morphological observation, sputter etching, induced deposition, and ion implantation [10–13]. The schematic principle diagram is shown in Figure 2, and representative application examples are shown in Figure 3.

 doi:10.20944/preprints202603.1683.v1

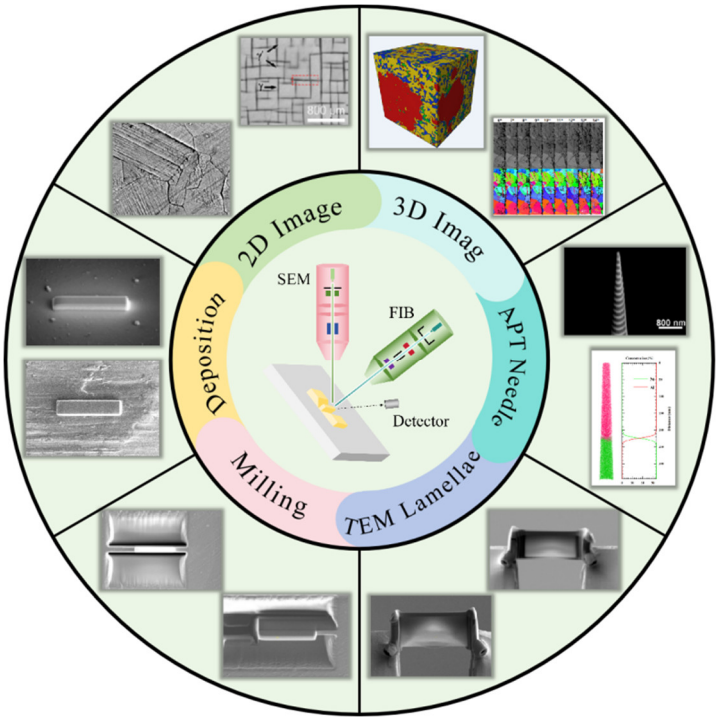

Figure 3. Examples of FIB-SEM micro-/nanofabrication processes and applications.

3. Applications of FIB-SEM in Morphological Characterization of Metallic Materials

3.1. 2D Morphological Characterization

Due to the etching effect of the high-energy ion beam, the ion beam causes specimen damage while collecting signals; the extent of this damage depends on the energy and intensity (accelerating voltage and beam current) of the ion beam [13–15]. Therefore, continuous imaging using the ion beam as the signal source is generally avoided. However, the GFIS-based helium/neon ion microscope [10,16,17], which operates on the quantum-mechanical tunneling effect, can be used for ultra-high-resolution imaging because of its low ion energy and minimal damage; its imaging contrast and surface detail are superior to those achieved by electron-beam imaging [6]. This is attributable to an extremely short de Broglie wavelength and a highly localized interaction volume, allowing ultimate surface imaging at sub-nanometer resolution [16] and clearly revealing true atomic-scale surface steps and morphologies with almost no subsurface information interference. Hlawacek et al. [17] used a helium ion microscope to study silver alloys confined to Pt(111) surfaces, directly visualizing single-atomic-layer-high steps between terraces and measuring the periodicity of hcp/fcc patterns formed in 2–3-layer-thick Ag/Pt alloy films, as shown in Figure 4 [17].

 doi:10.20944/preprints202603.1683.v1

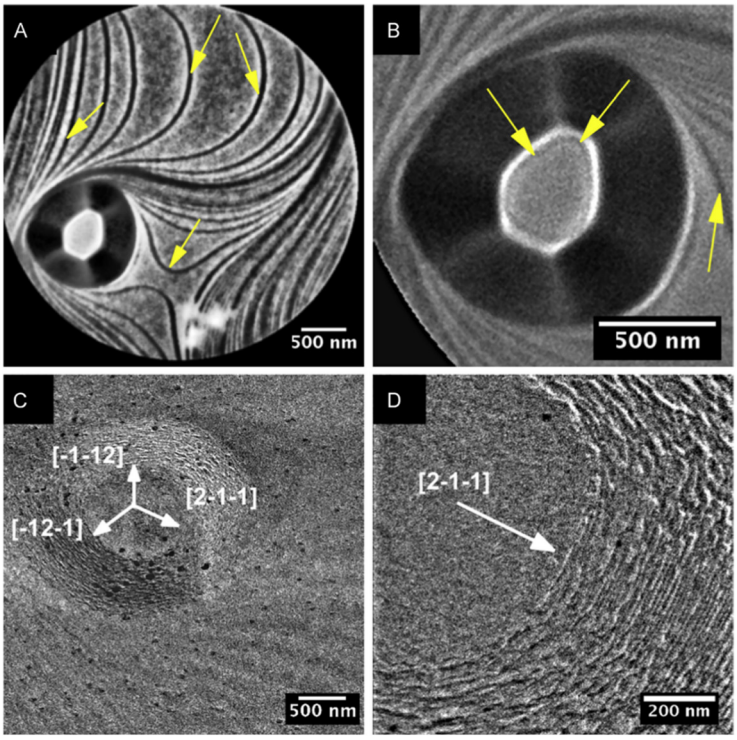

Figure 4. Helium ion focused ion beam system [17].

In addition, the strong interaction between ions and atomic nuclei endows ion-beam images with excellent material and grain contrast, allowing clear differentiation of grains with different orientations in polycrystalline materials and light-element components in composite materials. The positively charged incident ions naturally neutralize the surface charge of the specimen, enabling direct ultra-high-resolution imaging of insulators (e.g., ceramics, polymers, biological specimens) without prior conductive coating. Furthermore, the technique offers an exceptionally large depth of field and is free from edge-brightening artifacts, providing a more accurate representation of three-dimensional geometry. These characteristics make the helium/neon ion microscope an indispensable and powerful tool for exploring true surface structures at the nanoscale, especially the surface properties of insulating materials.

3.2. 3D Morphological Characterization

FIB-SEM three-dimensional tomography (FIB-SEM Tomography) has gradually become a core tool for resolving the three-dimensional spatial structure of metallic materials, owing to its unique capability to acquire true three-dimensional information from moderate microvolumes (10–1000 μm^3) at nanometer resolution [18–21]. In 2004, HOLZER et al. successfully reconstructed the three-dimensional structure of $BaTiO_3$. We also successfully employed a FIB-SEM dual-beam system to achieve slice-and-view 3D tomography, acquiring true three-dimensional (3D) information from moderate analysis volumes (10–1000 μm^3) of a given material at nanometer resolution, as shown in Figure 5.

 doi:10.20944/preprints202603.1683.v1

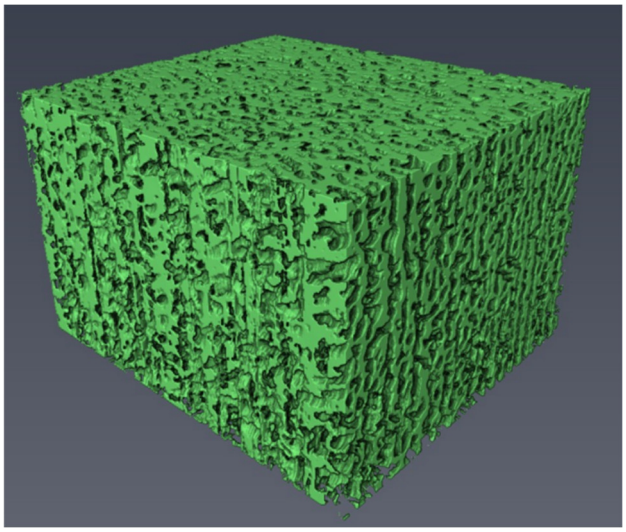

Figure 5. Three-dimensional imaging of nanoporous silver.

4. Applications of FIB-SEM in the Micro/Nanofabrication of Metallic Materials

Researchers have used FIB-SEM dual-beam systems, with real-time SEM monitoring, to precisely control key parameters such as ion species, energy, beam current, and dwell time, successfully achieving highly accurate three-dimensional controllable fabrication of platinum-wire nanocages, PtC nanotips, and self-assembled nanobubbles on gold films [22–27]. However, the most widespread uses of FIB-SEM in the field of metallic materials remain TEM specimen preparation, APT specimen preparation, and in situ compression experiments. These preparation techniques and the progress of their related analytical methods are introduced in detail in this section.

4.1. TEM Specimen Preparation

TEM enables nano/atomic-scale microstructural analysis of metallic materials. Under real-time SEM observation, FIB-SEM can be used to select regions of interest—such as crack tips, inclusions, and grain boundaries—and extract TEM specimens in either perpendicular or parallel orientations (Lift-out). Taking the perpendicular Lift-out method as an example, the procedure consists of eight steps: deposition, rough cutting, fine cutting, U-cutting, extraction, welding, final thinning, and cleaning. Steps 1 through 7 (deposition to final thinning) are typically performed at a machining voltage of 10–30 kV, while the cleaning step is typically carried out at 2–5 kV. A schematic diagram of the perpendicular Lift-out TEM specimen preparation process is shown in Figure 6.

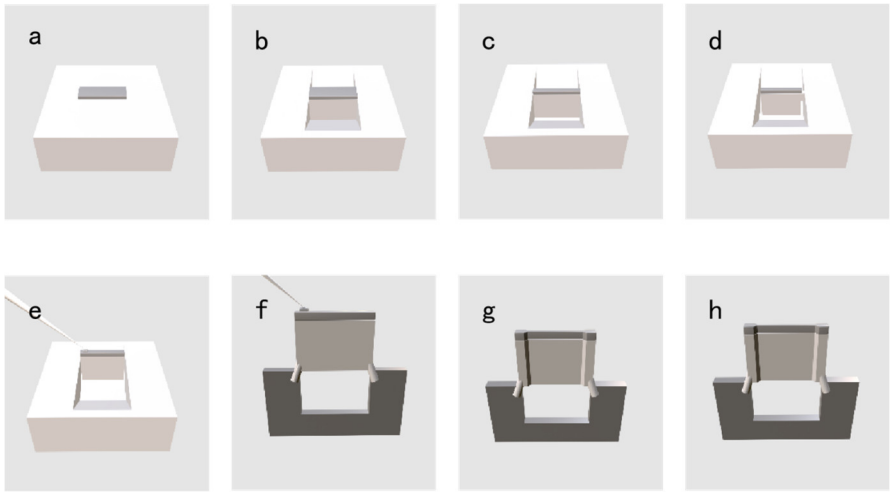

Figure 6. Three-dimensional schematic of TEM specimen preparation: (a) deposition; (b) coarse milling; (c) fine milling; (d) U-cutting; (e) lift-out; (f) welding; (g) final thinning; (h) cleaning.

 doi:10.20944/preprints202603.1683.v1

This technique continues to be updated and extended. We proposed a multi-voltage FIB-SEM Lift-out technique for extracting cross-sectional TEM specimens from diamond and Zr alloys [28,29]. TOMUS et al. [30], JUBLOT et al. [31], and WANG Xueli et al. [32] successfully developed FIB-SEM Lift-out techniques for preparing plan-view TEM specimens suitable for crack analysis. Deng et al. [33] proposed a thin-film-embedding-strengthened FIB (FeS-FIB) technique, based on FIB-SEM, to successfully extract TEM specimens from both spherical microparticles and nanosheet-type structures, and successfully analyzed the lattice structure of Ni and Fe double hydroxide (Ni,Fe-LDH) nanosheets.

4.2. APT Specimen Preparation

APT enables three-dimensional atomic-scale chemical compositional analysis of metallic materials. Under real-time SEM observation, FIB-SEM can be used to select regions of interest—including precipitate phases [34–41], grain boundaries [42–50], phase interfaces [51–53], and other regions of interest [54–56]—and extract APT specimens in either perpendicular or parallel Lift-out orientations. MILLER et al. [57,58] adapted the TEM specimen preparation concept to propose the Lift-out method for APT, which involves Pt protection, cut-and-extract, welding to microstubs, and final annular milling to achieve precise targeting of regions of interest. After continuous refinement of technical details by subsequent researchers [59,60], the Lift-out method has become the most universal standard approach for APT specimen preparation. A schematic diagram of the perpendicular APT Lift-out specimen preparation process is shown in Figure 7.

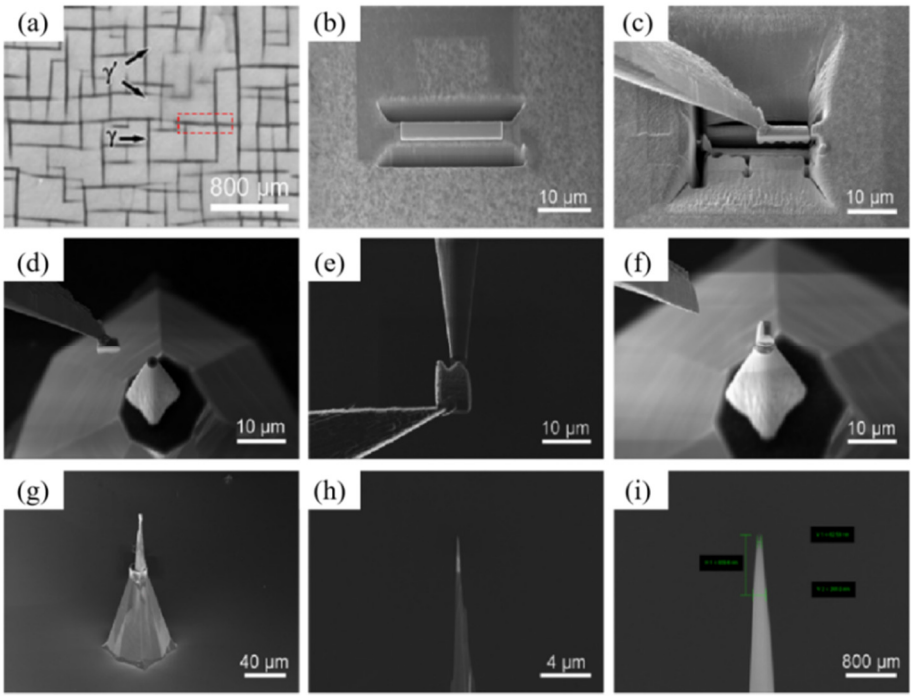

Figure 7. Standard lift-out procedure for FIB-prepared APT specimens: (a) Pt deposition; (b) coarse milling; (c) fine milling; (d) U-cutting; (e) lift-out; (f)-(g) welding; (h) final thinning; (i) cleaning.

These methods have been widely applied to metallic materials. Takahashi et al. [61] used APT analysis to investigate micron-scale spherical oxide inclusions in titanium-containing weld metal, revealing non-uniformly distributed multi-layered oxide shells of varying composition formed on an oxide core; the outermost oxide layer was rich in titanium and was surrounded by a manganese-depleted zone approximately 30–40 nm thick. Lee, Y. et al. [62] employed atom probe tomography (APT) to determine the temporal evolution of composition after heat treatment, in order to resolve the uncertainty in the Pt-Pd phase diagram, particularly the proposed miscibility gap. Woods et al. [63] built on this foundation to explore APT specimen preparation techniques for various metals,

 doi:10.20944/preprints202603.1683.v1

oxides, supported frozen liquids, and battery materials at low temperatures, successfully characterizing materials such as nickel-coated AAO membranes.

5. Other FIB-Based Correlative Characterization Techniques

Precise control of crystallographic orientation is also an important requirement for FIB-SEM micro/nanofabrication of metallic materials. GAO et al. [64] proposed an FIB-SEM-EBSD combined TEM specimen preparation technique to prepare TEM specimens of Widmanstätten structures in γ-TiAl alloys with specific zone axes, thereby successfully resolving the atomic structure of the special interface (Σ-11 CSL) between Widmanstätten and lamellar structures. COJOCARU-MIRÉDIN O et al. [65] proposed an FIB-SEM-EBSD-PPMS combined APT specimen preparation technique, enabling correlative characterization of crystal orientation, physical properties, and atomic-scale composition.

Time-of-flight secondary ion mass spectrometry (TOF-SIMS), which enables ppm- to ppb-level detection of all elements (from hydrogen H to transuranium elements) at solid material surfaces, has attracted the attention of materials researchers and has been integrated with FIB-SEM. Shin-ichi et al. [66] have realized the application of FIB-SEM-TOF-SIMS in all-solid-state batteries (ASSBs) using a Bi-ion-source FIB-SEM.

The mechanical behavior of metallic materials is also of major interest to researchers. UCHIC et al. [67] used micropillar compression to study the plastic flow behavior of pure nickel and superalloys at the micrometer scale. XUE et al. [68] proposed an FIB-SEM TEM specimen preparation technique based on in situ SEM tensile testing, studying the microstructural evolution in the heat-affected zone (HAZ) of laser-welded DP1180 dual-phase steel joints. KIENER et al. [69] proposed a quantitative in situ TEM tensile testing technique using FIB-prepared nano-specimens to study the plastic deformation mechanism of copper single crystals at the sub-micrometer scale (100–200 nm).

6. Conclusions and Outlook

This paper systematically reviews the latest research advances of FIB-SEM technology in the field of metallic materials science. The principles and basic functions of FIB-SEM are introduced, together with detailed descriptions of its applications in morphological characterization and TEM and APT specimen preparation, as well as its integration with other characterization techniques. Currently, FIB technology is advancing along two parallel trajectories: the concurrent development of multiple ion-source technologies (e.g., Ga^+, Xe^+, and other plasma sources) and their deep integration with multimodal characterization techniques. In the future, FIB technology is expected to combine with artificial intelligence and big data analysis to enable real-time, correlative measurements of multidimensional physical, chemical, and mechanical properties at the micro-scale, thereby providing powerful technical support for constructing a complete "materials genome" map.

Funding: This research received no external funding.

Data Availability Statement: The original contributions presented in this study are included in the article. Further inquiries can be directed to the corresponding author(s).

Conflicts of Interest: The authors declare no conflict of interest.

References

1. Sudraud, P.; Ben Assayag, G.; Bon, M. Focused-ion-beam milling, scanning-electron microscopy, and focused-droplet deposition in a single microcircuit surgery tool. Journal of Vacuum Science & Technology B: Microelectronics Processing and Phenomena **1988**, 6(1): 234-238.
2. Puretz, J.; Swanson, L.W. Focused ion beam deposition of Pt containing films. Journal of Vacuum Science & Technology B: Microelectronics and Nanometer Structures Processing, Measurement, and Phenomena **1992**, 10(6): 2695-2698.

 doi:10.20944/preprints202603.1683.v1

3. Van Den Heuvel, F.C.; Overwijk, M.H.F.; Fleuren, E.M.; et al. Focused-ion-beam-induced tungsten deposition for IC repair. Microelectronic Engineering **1993**, 21(1/2/3/4): 209-212.
4. Swanson, L.W. Use of the liquid metal ion source for focused beam applications. Applied Surface Science **1994**, 76/77: 80-88.
5. Preiß, E.I.; Merle, B.; Xiao, Y.; et al. Applicability of focused Ion beam (FIB) milling with gallium,neon,and xenon to the fracture toughness characterization of gold thin films. Journal of Materials Research **2021**, 36(12): 2505-2514.
6. Wang, R.M.; Duan, S.B.; Jiang N.S.; et al. Advanced characterization methods and technologies, China Machine Press, Beijing, China, 2024.
7. Burnett, T.L.; Kelley, R.; Winiarski, B.; et al. Large volume serial section tomography by Xe Plasma FIB dual beam microscopy. Ultramicroscopy **2016**, 161: 119-129.
8. Gholinia, A.; Curd, M.E.; Bousser, E.; et al. Coupled Broad Ion Beam-Scanning Electron Microscopy (BIB–SEM) for polishing and three dimensional (3D) serial section tomography (SST). Ultramicroscopy **2020**, 214: 112989.
9. Echlin, M.P.; Straw, M.; Randolph, S.; et al. The TriBeam system: Femtosecond laser ablation in situ SEM. Materials Characterization **2015**, 100: 1-12.
10. Li, P.; Chen, S.Y.; Dai, H.F.; et al. Recent advances in focused ion beam nanofabrication for nanostructures and devices: Fundamentals and applications. Nanoscale **2021**, 13(3): 1529-1565.
11. House, K.L.; Pan, L.; O'Carroll, D.M.; et al. Applications of scanning electron microscopy and focused ion beam milling in dental research. European Journal of Oral Sciences **2022**, 130(2): e12853.
12. Kim, C.S.; Ahn, S.H.; Jang, D.Y. Review: Developments in micro/nanoscale fabrication by focused ion beams. Vacuum **2012**, 86(8): 1014-1035.
13. Yuan, H.; Van De Moortèle, B.; Epicier, T. Accurate post-mortem alignment for Focused Ion Beam and Scanning Electron Microscopy (FIB-SEM) tomography. Ultramicroscopy **2021**, 228: 113265.
14. Sloyan, K.; Melkonyan, H.; Apostoleris, H.; et al. A review of focused ion beam applications in optical fibers. Nanotechnology **2021**, 32(47): 472004.
15. Boxleitner, W.; Hobler, G.; Klüppel, V.; et al. Simulation of topography evolution and damage formation during TEM sample preparation using focused ion beams. Nuclear Instruments and Methods in Physics Research Section B: Beam Interactions with Materials and Atoms **2001**, 175/176/177: 102-107.
16. Ward, B.W.; Notte, J.A.; Economou, N.P. Helium ion microscope: A new tool for nanoscale microscopy and metrology. Journal of Vacuum Science & Technology B: Microelectronics and Nanometer Structures Processing, Measurement, and Phenomena **2006**, 24(6): 2871-2874.
17. Hlawacek, G.; Jankowski, M.; Wormeester, H.; et al. Visualization of steps and surface reconstructions in Helium Ion Microscopy with atomic precision. Ultramicroscopy **2016**, 162: 17-24.
18. Fu, Q.Q.; Shan, Z.W. FIB-SEM dual-beam system and its partial applications. Journal of Chinese Electron Microscopy Society **2016**, 35(1): 81-89.
19. Holzer, L.; Indutnyi, F.; Gasser, P.H.; et al. Three-dimensional analysis of porous $BaTiO_3$ ceramics using FIB nanotomography. Journal of Microscopy **2004**, 216(Pt 1): 84-95.
20. Cantoni, M.; Holzer, L. Advances in 3D focused ion beam tomography. MRS Bulletin **2014**, 39(4): 354-360.
21. Taillon, J.A.; Pellegrinelli, C.; Huang, Y.L.; et al. Improving microstructural quantification in FIB/SEM nanotomography. Ultramicroscopy **2018**, 184: 24-38.
22. Wu, H.M.; Stern, L.A.; Chen, J.H.; et al. Synthesis of nanowires via helium and neon focused ion beam induced deposition with the gas field ion microscope. Nanotechnology **2013**, 24(17): 175302.
23. Shukla, N.; Tripathi, S.K.; Banerjee, A.; et al. Study of temperature rise during focused Ga ion beam irradiation using nanothermo-probe. Applied Surface Science **2009**, 256(2): 475-479.
24. Cui, A.J.; Li, W.X.; Shen, T.H.; et al. Thermally induced shape modification of free-standing nanostructures for advanced functionalities. Scientific Reports **2013**, 3: 2429.
25. Tuck, K.; Ellis, M.; Geisberger, A.; et al. FIB prepared TEM sample lift-out using MEMS grippers. Microscopy and Microanalysis **2004**, 10(S02): 1144-1145.
26. Zhao, L.R.; Cui, Y.M.; Li, J.Y.; et al. The 3D controllable fabrication of nanomaterials with FIB-SEM synchronization technology. Nanomaterials **2023**, 13(12): 1839.

 doi:10.20944/preprints202603.1683.v1

27. Haub, M.; Guenther, T.; Bogner, M.; et al. Use of PtC nanotips for low-voltage quantum tunneling applications. Micromachines **2022**, 13(7): 1019.
28. Qiao, Y.; Li, J.W.; Liu, G.; et al. Applications of FIB technique in the preparation of HRTEM samples for diamond/M(M = Cu,Al,Al N) composite materials. Journal of Chinese Electron Microscopy Society **2016**, 35(1): 53-57.
29. Qiao, Y.; Xu, Z.W.; Li, S.L.; er al. An integrated solution to FIB-induced hydride artifacts in pure zirconium. Micromachines **2024**, 15(8): 999.
30. Tomus, D.; Ng, H.P. In situ lift-out dedicated techniques using FIB-SEM system for TEM specimen preparation. Micron **2013**, 44: 115-119.
31. Jublot, M.; Texier, M. Sample preparation by focused ion beam micromachining for transmission electron microscopy imaging in front-view. Micron **2014**, 56: 63-67.
32. Wang, X.L.; Zhang, W.; Jia, Z.H.; et al. Preparation of parallel with the sample surface TEM sample using FIB technology. Journal of Chinese Electron Microscopy Society **2013**, 32(5): 420-425.
33. Deng, B.; Lei, L.; Wang, L.; et al. Extracting TEM lamellae from micro/nano particles through a thin film embedding strengthened FIB approach. Micron **2026**, 201..
34. Xiang, W.K.; Yang, N.T.; Li, X.P.; et al. 3D atomic-scale imaging of mixed Co-Fe spinel oxide nanoparticles during oxygen evolution reaction. Nature Communications **2022**, 13: 179.
35. Dumas, P.; Duguay, S.; Borrel, J.; et al.Atom probe tomography quantification of carbon in silicon. Ultramicroscopy **2021**, 220: 113153.
36. Yeli, G.; Strutt, V.C.I.; Auger, M.A.; et al. Characterisation of nano-scale precipitates in BOR60 irradiated T91 steel using atom probe tomography. Journal of Nuclear Materials **2021**, 543: 152466.
37. Akey, A.J.; Mathews, J.; Warrender, J.M. Maximum Ti concentrations in Si quantified with atom probe tomography (APT). Journal of Applied Physics **2021**, 129(17): 175701.
38. Jin, S.B.; Su, H.K.; Qian, F.; et al. Effects of atom probe analysis parameters on composition measurement of precipitates in an Al-Mg-Si-Cu alloy. Ultramicroscopy **2022**, 235: 113495.
39. Shah, S.; Thronsen, E.; De Geuser, F.; et al. On the use of a cluster identification method and a statistical approach for analyzing atom probe tomography data for GP zones in Al-Zn-Mg (-Cu) alloys. Microscopy and Microanalysis **2024**, 30(1): 1-13.
40. He, M.W.; Davids, W.J.; Breen, A.J.; et al. Quantifying short-range order using atom probe tomography. Nature Materials **2024**, 23(9): 1200-1207.
41. Stroud, R.S.; Al-Saffar, A.; Carter, M.; et al. Testing outlier detection algorithms for identifying early stage solute clusters in atom probe tomography. Microscopy and Microanalysis **2024**, 30(5): 853-865.
42. Hartshorne, M.; Leff, A.; Vetterick, G.; et al.Grain boundary plane measurement using transmission electron microscopy automated crystallographic orientation mapping for atom probe tomography specimens. Microscopy and Microanalysis **2023**, 29(3): 1018-1025.
43. Koelling, S.; Stehouwer, L.E.A.; Paquelet, W.B.; et al. Three-dimensional atomic-scale tomography of buried semiconductor heterointerfaces. Advanced Materials Interfaces **2023**, 10(3): 2201189.
44. Gemma, R.; Lu, Y.S.; Seils, S.; et al. Chemical characterization of $Mg_{0.25}Mn_{0.75}$-H(D) nanocomposites by atom probe tomography (APT). Journal of Alloys and Compounds **2022**, 896: 163015.
45. Licata, O.G.; Broderick, S.; Rocco, E.; et al. Dopant-defect interactions in Mg-doped GaN via atom probe tomography. Applied Physics Letters **2021**, 119(3): 032102.
46. Han, B.; He, F.; Xia, L.F.; et al. Effect of Ti/Al ratio on the elemental partitioning in the face-centered cubic-based γ-γ′ dual-phase high entropy alloy studied by atom probe tomography. Frontiers in Materials **2022**, 9: 806237.
47. Ikehata, H.; Maeshima, T.; Oh-Ishi, K.; et al. Grain boundary segregation behavior and thermodynamic analysis based on CALPHAD method for B added high carbon steel. Materials Transactions **2024**, 65(5): 568-575.
48. Lee, Y.; Stender, P.; Eich, S.M.; et al. Probing the miscibility gap of the Pt–Pd binary system by atom probe tomography. Microscopy and Microanalysis **2022**, 28(4): 1385-1395.
49. Toyama, T.; Zhao, C.; Yoshiie, T.; et al. Radiation-enhanced diffusion of copper in iron studied by three-dimensional atom probe. Journal of Nuclear Materials **2021**, 556: 153176.

 doi:10.20944/preprints202603.1683.v1

50. Eriksson, G.; Hulander, M.; Thuvander, M.; et al. Silica-embedded gold nanoparticles analyzed by atom probe tomography. Microscopy and Microanalysis **2025**, 30(6): 1036-1046.
51. Jenkins, B.M.; Haley, J.; Moody, M.P.; et al. APT and TEM study of behaviour of alloying elements in neutron-irradiated zirconium-based alloys. Scripta Materialia **2022**, 208: 114323.
52. Takahashi, J.; Kisaka, Y.; Kawakami, K.; et al. Atomic-scale analysis of oxide inclusion in weld metal using atom probe tomography. Metallurgical and Materials Transactions A **2022**, 53(5): 1693-1703.
53. Cojocaru-Mirédin, O.; Yu, Y.; Köttgen, J.; et al. Atom probe tomography: A local probe for chemical bonds in solids. Advanced Materials **2024**, 36(50): 2403046.
54. Takahashi, J.; Kawakami, K.; Sakiyama, Y.; et al. Atomic-scale observation of hydrogen trap sites in bainite–austenite dual-phase steel by APT. Materials Characterization **2021**, 178: 111282.
55. Zhao, Y.B.; Li, Z.; Wang, J.P.; et al. Tensile properties and fracture mechanism of strain rate brittleness on quenched cold-rolled carbon steel. Steel Research International **2022**, 93(1): 2100361.
56. Tegg, L.; Mccarroll, I.E.; Kim, S.H.; et al. Analysis of water ice in nanoporous copper needles using cryo atom probe tomography. Microscopy and Microanalysis **2025**, 30(6): 1195-1204.
57. Miller, M.K.; Russell, K.F.; Thompson, G.B. Strategies for fabricating atom probe specimens with a dual beam FIB. Ultramicroscopy **2005**, 102(4): 287-298.
58. Miller, M.K.; Russell, K.F.; Thompson, K.; et al. Review of atom probe FIB-based specimen preparation methods. Microscopy and Microanalysis **2007,** 13(6): 428-436.
59. Kiener, D.; Zhang, Z.; Šturm, S.; et al. Advanced nanomechanics in the TEM:Effects of thermal annealing on FIB prepared Cu samples. Philosophical Magazine **2012**, 92(25/26/27): 3269-3289.
60. Xiao, Y.; Wehrs, J.; Ma, H.; et al. Investigation of the deformation behavior of aluminum micropillars produced by focused ion beam machining using Ga and Xe ions. Scripta Materialia **2017**, 127: 191-194.
61. Takahashi, J.; Kisaka, Y.; Kawakami, K.; et al.. Atomic-Scale Analysis of Oxide Inclusion in Weld Metal Using Atom Probe Tomography. Metallurgical and Materials Transactions A **2022**, 53(5), 1693-1703.
62. Lee, Y.; Stender, P.; Eich, S.M.; et al. Probing the Miscibility Gap of the Pt–Pd Binary System by Atom Probe Tomography. Microscopy and Microanalysis **2022**, 28(4), 1385-1395.
63. Woods, E.V.; Singh, M.P.; Kim, S.H.; et al. A Versatile and Reproducible Cryo-sample Preparation Methodology for Atom Probe Studies. Microscopy and Microanalysis **2023**, 29(6), 1992-2003.
64. Gao, Z.T.; Hu, R.; Gao, X.Y.; et al. Characterization of the Widmanstätten structure in γ-TiAl alloy using an EBSD-FIB-TEM combined process. Scripta Materialia **2023**, 222: 115001.
65. Cojocaru-Mirédin, O.; Devaraj, A.; Editors, G. Correlative microscopy and techniques with atom probe tomography:Opportunities in materials science. MRS Bulletin **2022**, 47(7): 680-687.
66. Iida, S.; Fisher, G.L.; Miyayama, T. Sample processing by Bi-FIB for in situ TOF-SIMS imaging of buried interfaces. Surface and Interface Analysis **2022**, 55(3), 209-214.
67. Uchic, M.D.; Dimiduk, D.M.; Florando, J.N.; et al. Sample dimensions influence strength and crystal plasticity. Science **2004**, 305(5686): 986-989.
68. Xue, J.L.; Guo, W.; Yang, J.; et al. In-situ observation of microcrack initiation and damage nucleation modes on the HAZ of laser-welded DP1180 joint. Journal of Materials Science & Technology **2023**, 148: 138-149.
69. Kiener, D.; Minor, A.M. Source truncation and exhaustion:Insights from quantitative in situ TEM tensile testing. Nano Letters **2011**, 11(9): 3816-3820.